Dynamic association of calcium channel subunits at the cellular membrane

Andreas Voigt
Romy Freund
Jennifer Heck
Markus Missler
Gerald J. Obermair
Ulrich Thomas
Martin Heine

Dynamic association of calcium channel subunits at the cellular membrane

Andreas Voigt,[a,†] Romy Freund,[b,†] Jennifer Heck,[b] Markus Missler,[c] Gerald J. Obermair,[d] Ulrich Thomas,[e] and Martin Heine[b,f,]*

[a]Otto-von-Guericke-University of Magdeburg, Lehrstuhl Systemverfahrenstechnik, Universitätsplatz 2, Magdeburg D-39106, Germany
[b]Leibniz-Institute of Neurobiology, Research Group Molecular Physiology, Brenneckestrasse 6, Magdeburg D-39118, Germany
[c]Westfälische Wilhelms-University, Institute of Anatomy and Molecular Neurobiology, Vesaliusweg 2, Münster 48149, Germany
[d]Medical University Innsbruck, Division of Physiology, Department of Physiology and Medical Physics, Schöpfstrasse 41, Innsbruck 6020, Austria
[e]Leibniz-Institute of Neurobiology, Department Neurochemistry, Brenneckestrasse 6, Magdeburg D-39118, Germany
[f]Otto-von-Guericke-University Magdeburg, Center for Behavioral Brain Sciences (CBBS), Universitätsplatz 2, Magdeburg D-39106, Germany

Abstract. High voltage gated calcium channels (VGCCs) are composed of at least three subunits, one pore forming α_1-subunit, an intracellular β-variant, and a mostly extracellular $\alpha_2\delta$-variant. Interactions between these subunits determine the kinetic properties of VGCCs. It is unclear whether these interactions are stable over time or rather transient. Here, we used single-molecule tracking to investigate the surface diffusion of α_1- and $\alpha_2\delta_1$-subunits at the cell surface. We found that $\alpha_2\delta_1$-subunits show higher surface mobility than α_1-subunits, and that they are only transiently confined together, suggesting a weak association between α_1- and $\alpha_2\delta_1$-subunits. Moreover, we observed that different α_1-subunits engage in different degrees of association with the $\alpha_2\delta_1$-subunit, revealing the tighter interaction of $\alpha_2\delta_1$ with $Ca_V1.2 > Ca_V2.2 > Ca_V2.1 > Ca_V3.2$. These data indicate a distinct regulation of the $\alpha_1/\alpha_2\delta_1$ interaction in VGCC subtypes. We modeled their membrane dynamics in a Monte Carlo simulation using experimentally determined diffusion constants. Our modeling predicts that the ratio of associated α_1- and $\alpha_2\delta_1$-subunits mainly depends on their expression density and confinement in the membrane. Based on the different motilities of particular $\alpha_1/\alpha_2\delta_1$-subunit combinations, we propose that their dynamic assembly and disassembly represent an important mechanism to regulate the signaling properties of VGCC. [DOI: 10.1117/1.NPh.3.4.041809]

1 Introduction

Transient activation of high voltage gated calcium channels (VGCCs) is a critical and widespread cellular process. For example, VGCC activation is essential for vesicular transmitter release in neurons, excitation contraction coupling in muscle cells, and induction of intracellular signaling cascades via Ca^{2+}-influx in many excitable cells.[1] VGCCs are able to open and close so rapidly that, in conjunction with efficient Ca^{2+}-buffering and clearance, changes in Ca^{2+}-concentration can be confined to the nanometer range. Such a highly localized VGCC function plays an important role at neuronal synapses where the positioning of presynaptic VGCCs relative to Ca^{2+}-effectors for synaptic vesicle (SV) fusion is crucial for neurotransmitter release. At fast synapses, activation of a single VGCC may trigger release if it is in close proximity to a fusion-competent SV.[2–4] Consistent with such a scenario, we reported recently that the number and mobility of VGCCs within active zones are relevant parameters for the synaptic function.[5] It remained unclear, however, if the subunit-based molecular composition of VGCC affects these dynamic parameters.

VGCCs are composed of three principal subunits: the pore forming α_1-subunit which determines the type of Ca^{2+} channel, and two auxiliary subunits, an intracellular β-subunit and a membrane-anchored $\alpha_2\delta$-subunit with a large, highly glycosylated extracellular domain. It has been widely assumed that the three subunits within a VGCC display a stoichiometry of $1:1:1$ and that the composition remains stable over time.[6,7] Several distinct β- and $\alpha_2\delta$-isoforms and splice variants are encoded in most vertebrate genomes, and changes in the combination of α_1, β- and $\alpha_2\delta$-subunits within a particular VDCC have a substantial impact on kinetic properties and trafficking.[7–9] For example, exchanging β-subunits altered the inactivation properties of presynaptic $Ca_V2.1$ and $Ca_V2.2$ and changed presynaptic transmitter release.[10] While $\alpha_2\delta$-subunits can also alter the voltage-dependent channel inactivation,[11,12] their major function is their ability to promote channel trafficking and to tune the number of synaptic VGCC.[8,13] The latter property may account for pathological conditions characterized by an increase of surface expressed calcium channels.[9,14] In addition, $\alpha_2\delta$-subunits may assume VGCC-independent functions during synaptogenesis by their interaction with extracellular proteins like thrombospondins.[15,16] Genomic aberrations of $\alpha_2\delta_1$-subunits have been reported to cause epilepsy and intellectual disabilities as well as hyperinsulinism in humans caused by deletion of the CD36 gene.[17]

The extracellular von Willebrand A domain and cache domains of $\alpha_2\delta$-subunits have been implicated in the physical interaction with the first three segments of the α_1-subunit.[18–20] Moreover, multiple glycosylation sites of the $\alpha_2\delta$ appear to

*Address all correspondence to: Martin Heine, E-mail: martin.heine@lin-magdeburg.de

†These authors contributed equally.

contribute to the association with α_1-subunits.[21] The affinities between α_1- and $\alpha_2\delta$-subunits, however, appear rather weak as their association in the channel complex is sensitive to low-stringency detergents such as digitonin.[22,23] Consequently, the abundance of $\alpha_2\delta$ in a proteomic approach aimed at identifying core proteins of the calcium channel complex was below 10% compared to α_1- or β-subunits.[23] A direct interaction of α_1- and $\alpha_2\delta$-subunits via a transmembrane domain of the δ-domain was proposed,[24] but identification of a glycosylphosphatidylinositol (GPI)-anchor present in all $\alpha_2\delta$-subunits[25] argues against a transmembrane interaction. Here, we used single-particle tracking methods to investigate the surface dynamics and putative association between α_1- and $\alpha_2\delta$-subunits. We focused mostly on $Ca_V2.2$ and $\alpha_2\delta_1$-subunits because of their prominent role in the induction and expression of chronic pain in the peripheral nervous system.[14,26]

2 Materials and Methods

2.1 Cell Culture

HEK293-T cells and tsA-201 cells (large SV40 T-antigen transformed HEK293) were grown in DMEM supplemented with 10% fetal calf serum (FCS), 1% antibiotic/antimycotic, and 1% L-glutamine. tsA-201 cells stably expressing rat $Ca_V2.2$ (in pcDNA6, blasticidin resistence, GenBank No. AF055477), rat β_3 (in pcDNA3.1, reocin resistence), and rat $\alpha_2\delta_1$ (in pcDNA3, hygromycin resistence, GenBank No. AF286488) were a gift from D. Lipscombe.[27] All cells were cultured in 5% CO_2 and a humidity of 95% at 37°C. All supplemented cell culture media were sterile filtrated (0.22 μm pore size) and kept at 4°C until use. Cells were transfected for 48 h before experiments using transfection reagencies based on cationic lipids (FuGENE®HD Transfection Reagent, Roche).

Dissociated neuronal cultures were prepared from hippocampus as described before[5] and transfected with calcium channel constructs at 3 to 5 days-in-vitro (DIV). For fluorescence recovery after photobleach (FRAP) and single-particle tracking (SPT) experiments, cultures of 14 to 21 DIV were mounted in an open chamber perfused with extracellular solution as specified below and imaged for up to 20 min at 36°C/RT.

2.2 Molecular Biology

$Ca_V2.2::HA$ expression construct was modified from rat α_{1B}-subunit (Q02294; kindly provided by Gerald Zamponi) by PCR to insert the HA-epitope (YPYDVPDYA) into the extracellular loop between the fifth and sixth transmembrane domain after F^{254}, resulting in the duplication of C^{253}/F^{254} after the epitope ($HKACF^{254}$—HA-epitope—$C^{253}FPNS$). Specifically, two $\alpha1B$-PCR fragments were generated using the following pairs of primers: (1) ratN-NotI_fw: cta ggc ggc cgc tat ggg ggc ac/ ratN-5P(HA) RV_rev: P-gtc ata tgg ata gaa gca ggc ctt atg gaa ttt g and (2) ratN-5P(HA)RV fw: P-gtc cct gat tac gcc tgc ttc ccc aac agc aca g/ratN-syn_rev and ccc gta cgc ggg cct cga tgt ctt gcg. With the first and second halves of the epitope-encoding sequence included in the forward and reverse ratN-5P(HA) primers and NotI or BswI sites included in the outer primers, respectively, the two fragments were tail-to-head ligated and thereafter used to replace the respective NotI-BswI fragment in the original rat $Ca_V2.2$ construct.

Similarly, $Ca_V2.2::GFP$ was based on rat sequence (CAC1B_RA) and generated by inserting eGFP with short linkers coding for restriction sites into the last P-loop between amino acids 1672/1673 by site-directed mutagenesis. The resulting sequence was confirmed by sequencing as ... MQVFGNIALDDGTSINRHNNFRTFLQALMLLFRS-ATGEAWHEIMLSCLGNRACDP<Gly-Thr-eGFP-Thr-Glu-Gly-Thr>HANASECGSDFAYFY ... N-terminal GFP-tagged $Ca_V3.2$ was provided by E. Bourinet (Montpellier, France), and generation of GFP-tagged $Ca_V1.2$ as well as of $\alpha_2\delta_1$-subunit with a double HA-epitope inserted after the predicted signal peptide into a rabbit cDNA (Genbank: M21948; expressed from neuronal β-actin promoter) were previously described.[28] To allow the use of different labeling antibodies, we also exchanged the N-terminal HA-tag of the $\alpha_2\delta_1$-subunit to an FLAG epitope at the same position.

2.3 Electrophysiology

Whole-cell recordings from HEK cells were performed 48 to 72 h posttransfection for different combinations of Ca_V2.-subunits, using an EPC 10 amplifier (HEKA, Germany) controlled by the PatchMaster software (HEKA). Patch pipettes were pulled from borosilicate glass capillaries with a resistance of 2 to 5 MΩ. The internal solution contained in mM: 130 CsCl, 3 $MgCl_2$, 0.66 $CaCl_2$, 11.7 EGTA, 10 HEPES (pH 7.3), and 305 mOsm. Prior to experiments, fresh ATP solution was added to a final concentration of 2 mM and the pH was adjusted to 7.3 with CsOH. The extracellular solution contained in mM: 140 NaCl, 10 $BaCl_2$, 1 $MgCl_2$, 10 HEPES, 10 D-(+)-glucose, pH 7.4 was adjusted with NaOH. Recordings were performed at room temperature (22 to 25°C) under constant perfusion with extracellular solution. Barium currents were recorded in whole-cell mode using the p/4 protocol to subtract leak currents. Data were analyzed using FitMaster (HEKA) and IGOR Pro (WaveMetrics) software. The stimulus protocols were designed within the PatchMaster Pulse Generator.

2.4 Immunocytochemistry

Primary antibodies were applied to live or fixed HEK293 or COS-7 cells to distinguish between surface and total populations of channel subunits. Live cell labeling was done in culture medium for 15 to 30 min at 37°C. Cells were fixed with 4% paraformaldehyde (PFA) in phosphate buffered salt solution (PBS) for 5 min, then washed and permeabilized for 2 min with 0.3% TritonX/PBS. Nonspecific immune reactivity was blocked by washing cells three times for 10 min with a washing buffer containing 10% FCS, 25 mM Glycin, and 2% bovine serum albumin (BSA) in PBS. Primary and secondary antibodies were applied consecutively for 1 h at RT. After additional washing steps, cells were mounted on glass slides with Mowiol (Sigma). The following primary antibodies were used: polyclonal rabbit anti-GFP antibody 1:200 (Invitrogen; A6455), monoclonal mouse anti-HA antibody (1:200; Covance; MMS-101P); secondary fluorescently labeled antibodies included: anti-mouse ATTO 647N 1:200 (Sigma-Aldrich, 50185-1ML-F) and anti-rabbit Abberior STAR 580 1:200 (Abberior; 2-0012-005-8) or Alexa 488 (Thermo-Fisher Scientific, A-11034).

2.5 Imaging and Colocalization Analysis

Fluorescence labeling of cells was examined by either using a conventional epifluorescence microscope coupled to a CCD camera (ImagerA2 microscope, Zeiss, coupled to a CoolSnap

Myo CCD-camera, Roper Scientific) or by use of an stimulated emission depletion (STED) microscope (SP5, Leica, Germany). To determine the colocalization of extra- or intracellularly GFP-tagged $Ca_V2.2$ and $\alpha_2\delta_1 :: HA$-subunits, Z-stacks were recorded using a Leica TCS SP5 2-channel STED microscope equipped with an inverted microscope DMI 6000 and a 100×-STED objective (HCX PL APO 100×, 1.4 NA oil STED, Leica Microsystems). The fluorophores used, Abberior STAR580 and Atto647N, were sequentially excited with pulsed-diode lasers (PicoQuant) at 531 and 635 nm. The fluorescence signals were detected with avalanche photodiodes (Perkin Elmer Inc.) through BL HC 607/36 (Abberior STAR580) and ET BP 670/30 (Atto647N) emission filters separated by a dichroic beam splitter at 650 nm. Depletion was performed at 730 nm for Abberior STAR580 and at 750 nm for Atto647N with a titanium sapphire laser (Chameleon ultra II, Coherent). The stacks were acquired at a resolution of 12 bits and in 1024×1024 pixel format with a pixel size of 25.2 nm (due to 6 × zoom). The scan speed was set to 700 Hz by using 48× line averaging.

Maximal intensity projections of the STED stacks were generated and the background was subtracted with a rolling ball radius of 10 pixels using ImageJ (version 1.44). The colocalization was analyzed from 512×512 pixel image sections with the software OpenView (provided by Dr. N. Ziv, Tel Aviv, Israel). Here, fluorescent clusters positive for the GFP-tagged $Ca_V2.2$ were determined by centering 10×10 pixel boxes around the local fluorescent maximum. The colocalization of fluorescent spots was defined by matching pixel boxes within a radius of 4 pixels. The matched area was set to overlap at least a 4×4 pixels region to be considered as colocalized.

2.6 Fluorescence Recovery After Photobleach Experiments

Hippocampal cultures were imaged on an inverted fluorescence microscope (Axio Observer D1, Zeiss) using a heated imaging chamber (TC-344B, Warner Instruments) and an EMCCD camera (Evolve 512, Photometrics) controlled by MetaMorph Imaging software. The FRAP laser (DL-473, Rapp Opto-electronics) was coupled to a point scanning device controlled by the software via a UGA40 control unit (Rapp Opto-electronics). The FRAP laser was pointed at up to 10 regions of interest (ROI) within one experiment with a dwell time per ROI of 10 ms. About 50 to 100 images were acquired before photobleach followed by an additional image acquisition for the next 5 min after photobleach. Image sequences were analyzed using MethaMorph and GraphPad Prism5 software. The recovery rate was determined after background subtraction and bleach correction. The relative recovery rate was calculated by the ratio of ROI fluorescent intensity for every time point versus the intensity before (set to 100%) and immediately after photobleach (set to 0%).

2.7 Single-Particle Tracking with Quantum Dots

GFP- or HA-tagged constructs were labeled with QDs precoated on monoclonal mouse anti-GFP (clone 7.1 and 13.1, 11814460001, Roche) or rat anti-HA antibody (clone 3F10, Roche), respectively. Precoating of QDs was performed as described before.[29] In brief, 1 μl of 1 μM QD-655 conjugate against mouse or rat [goat F(ab')2 anti-mouse or anti-rat IgG conjugate, Molecular Probes] was precoated with the corresponding antibody (0.5 μg, ~0.5 μl) in 7.5 μl PBS for 15 min and

blocked with 1 μl Casein solution (Vector Laboilities) for an additional 15 min. Precoated QDs were used to label surface-expressed, epitope-tagged subunits of transfected cells at a final concentration of 0.1 to 0.01 nM for 1 to 5 min at 37°C. Labeled cells were washed three times for 1 min in extracellular solution containing 0.5% BSA before imaging.

HEK cells and primary hippocampal neurons were mounted in an open chamber (Ludin chamber, Basel, Swiss) and used for imaging experiments in an extracellular solution of the following composition in mM: 145 NaCl, 10 Glucose, 10 HEPES, 5 KCl, 2 $CaCl_2$, 2 $MgCl_2$. Imaging of QDs was conducted at an inverted Zeiss microscope (AxioObserver) equipped with an EMCCD camera (Evolve™ 512, Photometrics) using a 100× 1.4 NA objective. Fluorescence of QD was excited by a Xenon lamp using excitation filter HC 531/40 (Semrock), and emitted fluorescence was acquired through a HC 655/15 bandpass filter (Semrock). Images were acquired at video rate (30Hz) using MetaMorph stream acquisition software.

Tracking of QDs was performed by the use of custom-made software.[30] Trajectories of single QDs were reconstructed by allowing reconnection of positions within two pixels distance to the previous image. The mean square displacement (MSD) was calculated and plotted over time for reconnected trajectories of at least 100 frames. Diffusion coefficients were calculated by linear fit of the first four points of the MSD plots versus time. The diffusion coefficient and confinement index were calculated using custom software as described in Ref. [31].

2.8 Single-Particle Tracking Photoactivated Localization Microscopy (Sptpalm) Imaging

A TIRF set-up was based on an inverted microscope (IX71 Olympus, Germany) and equipped with a manual TIRF illuminator arm and TIRF objective (100×, NA1.49). Generation and use of the mEOS2-tagged $Ca_V2.2$ construct was described in a previous work.[5] The tag was inserted on the same position as GFP in the N-terminus. Briefly, we used laser diodes to photoconvert and excite the fluorophore by continuous illumination of the probe with a 405-nm laser (2% to 5% of 100 mW) and a 561-nm laser (25% to 40% of 100 mW). Images were acquired by an EM-CCD camera (Andor, EMCCD, IXon Ultra). The green fluorescence of mEOS2 (exitation at 488 nm) was used to identify transfected cells. Images were recorded at 30 Hz for up to 4000 frames. We used a 1.6 magnification lens to reduce the pixel size to 100×100 nm^2.

2.9 Image Analysis

Localization and trajectory reconnection of mEOS2 signals was performed by the use of a wavelet based algorithm,[32] implicated in the super resolution software application from MetaMorph. Trajectories of mEOS2-tagged molecules were reconstructed by a simulated annealing algorithm,[33] taking into account molecule localization and total intensity. It has been described that mEOS2 molecules can show blinking-like behavior.[34] To avoid false reconnections between trajectories, all subtrajectories of mEOS2 were analyzed as individual trajectories. The dynamic behavior of single molecule was computed from the MSD curves for all trajectories of at least 8 frames. Diffusion coefficients were calculated by linear fit of the first four points of the MSD plots. MSD plots of immobilized molecules (on fixed samples) revealed that under our imaging conditions $D \geq 0.001$ $\mu m^2/s$ can be considered to be mobile. This threshold

was used for QD analysis as well. Trajectories from QD-labeled subunits were used to calculate the confinement and explored membrane surface area as described.[35]

3 Monte Carlo Simulation of Subunit Interactions

The simulation has been implemented in MATLAB R2015b. The random number generation was carried out using different pseudorandom number algorithms (RNGs) such as "mersenne twister," "combined multiple recursive," and "multiplicative lagged fibonacci." Within the statistical averages from 20 independent runs, all results were similar from the different RNGs in the framework of calculated mean values and error variances. Typical run times of simulations were on the order of a few minutes.

3.1 Statistics

Analysis of differences in data distributions or mean values was done by the use of GraphPad Prism software, using statistical tests as indicated in the legends. Data are shown either as median and an interquatril range, or as mean $\pm$ SEM. Significance levels are given as *, $p < 0.05$; **, $p < 0.005$; and ***, $p < 0.0005$; n.s., nonsignificant.

4 Results

4.1 Functional Characterization of Extracellularly Tagged Ca^{2+} Channel Subunits

Live imaging of endogenous VGCCs ideally requires surface labeling with antibodies against an extracellular domain of α_1- or $\alpha_2\delta$-subunits. Despite numerous attempts by several groups, this strategy has not yet been successful, presumably because of the small size of the extracellular domains and blocking of normal channel function of α_1-subunits, and/or limited antigenicity due to extensive glycosylation of $\alpha_2\delta$-subunits.[21] Using an alternative strategy, surface labeling of VGCC has been achieved by insertion of small epitope tags in an outer loop of the pore forming α_1-subunit of Ca$_V$1.2 and Ca$_V$2.2 channels without major impact on channel traffic and function.[36–41] However, a similar approach was not successful for the Ca$_V$2.1 channel,[42] a serious drawback as Ca$_V$2.1 is the predominant variant in most excitatory synapses. In this study, we, therefore, tested additional positions in the outer loops of Ca$_V$2.1 and Ca$_V$2.2 for the insertion of HA- and GFP-epitopes. The successful positions for both tags in the pore-forming subunit of Ca$_V$2.2 are indicated in Fig. 1(a). Subunits carrying an epitope were expressed on the surface of heterologous HEK293 cells and reliably detected by live labeling using anti-HA or anti-GFP antibodies [Fig. 1(b)]. We then tested the expression of the tagged Ca$_V$2.2 constructs in cultured hippocampal or DRG neurons, but obtained very heterogeneous results with respect to a detectable surface population which could not be improved by coexpression of $\alpha_2\delta_1$-subunit (data not shown). Problems with reliable neuronal surface expression of extracellularly tagged VGCCs are in contrast with the successful targeting of pore-forming subunits where the epitope is placed on its cytoplasmic N-terminus.[5] For our investigation of the VGCC subunit interaction and surface dynamics, we, therefore, chose the heterologous cell expression system.

To characterize the extracellularly tagged Ca$_V$2.2 variants electrophysiologically, we performed whole-cell recordings of
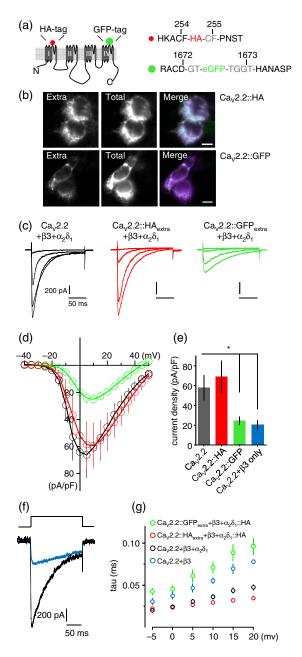

Fig. 1 Functional characterization of extracellular tagged constructs of the Ca$_V$2.2 channel. (a) The position of the two tagging positions is indicated in the sketch of the α_1-subunit of the channel, the inset position is given for both the HA-tag and GFP-tag plus the flanking linkers (in gray). (b) Immune fluorescent labeling of the constructs expressed in HEK cells for surface expressed channel population (live labeling, extra) and total channel population after fixation of the cells (total). (c) Representative barium currents evoked by depolarizing potential steps from -90 mV holding potential to -20; -10; 0; 10 mV for 200 ms and stepping back to 90 mV. (d) Current voltage relationship for the WT, Ca$_V$2.2 :: HA and the Ca$_V$2.2 :: GFP construct, note the clear differences in the current density as well as minor changes in the maximal activation voltage. (e) Quantification of the current density for WT Ca$_V$2.2/Ca$_V$2.2 :: HA/Ca$_V$2.2 :: GFP and WT Ca$_V$2.2 expressed with the β_3-subunit only. (f) Illustrating example for the voltage-dependent inactivation for a test potential to 10 mV for the WT Ca$_V$2.2 (black) and the WT Ca$_V$2.2 expressed with the β_3-subunit only (blue). (g) Quantification of the time constant for voltage-dependent inactivation at different test potentials, the different combinations are given in the legend. The data are from 5 to 20 cells for each combination of channel subunits. Statistical differences are determined by one-way ANOVA test followed by a *posthoc* Bonferroni-test. Data given as mean $\pm$ SEM, * $=p < 0.05$.

transfected HEK293 cells, coexpressing subunits α_{1B} with and without epitope tags, β_3, and $\alpha_2\delta_1$ [Figs. 1(c)–1(g)]. Representative traces [Fig. 1(c)], I/V-curves [Fig. 1(d)], and maximal current densities [Fig. 1(e)] were not different between the WT and HA-tagged channels. Expression of the GFP-tagged $Ca_V2.2 :: GFP$, however, showed a >50% reduction in current density compared to $Ca_V2.2$ or $Ca_V2.2 :: HA$ [Fig. 1(e)]. Interestingly, the $Ca_V2.2 :: GFP/\beta_3/\alpha_2\delta_1$ channel complex containing such a large epitope still showed similar current densities to WT $Ca_V2.2/\beta_3$ VGCCs without coexpressed $\alpha_2\delta_1$-subunits.

We next probed activation and steady-state-inactivation properties of our tagged $Ca_V2.2$ and compared these parameters to barium currents recorded from a stable $Ca_V2.2$ cell line[27] with no tags on α_1- or $\alpha_2\delta_1$-subunits (Table 1). Since the association of $\alpha_2\delta_1$ with α_1-subunit not only promotes surface expression, but also influences the time course of voltage-dependent inactivation,[11] we tested this parameter for all three channel constructs at different potentials. Similar to their current densities, the HA-tagged ($Ca_V2.2 :: HA$) channel was not significantly different from the WT channel. The extracellular GFP-tagged $Ca_V2.2$ ($Ca_V2.2 :: GFP_{extra}$) showed a slower inactivation, comparable to WT-$Ca_V2.2$ channel expressed without $\alpha_2\delta_1$ [Figs. 1(c) and 1(e)]. Coexpression of the α_1-subunit with the β_3 alone led to similar current kinetics as seen with the $Ca_V2.2 :: GFP_{extra}$ [Fig. 1(d)]. Thus, both current density and inactivation time course indicate that the large insert of an extracellular GFP limits the association of the $\alpha_2\delta_1$-subunits with the $Ca_V2.2$ channel.

To finally characterize the effect of the binding of Quantum dot (QD)-coupled-antibodies on VGCC function, important for our study of surface dynamics (see below), we compared the kinetic properties of WT and tagged channels under addition of anti-HA and anti-GFP antibodies (Table 1). The extracellular HA- and GFP-tagged $Ca_V2.2$ channels showed a shift of 5 mV to more positive potentials. The addition of tag specific antibodies also changed the steady-state inactivation of the tagged channel in comparison to nontagged channels (Table 1). The bias in the functional properties might have an impact on the proper function of $Ca_V2.2$ channels in neuronal membrane compartments, specifically the synapse. Nevertheless, we assume that in HEK cells the majority of channels will be in steady-state inactivation. Thus, surface mobility of calcium channels in

the membrane of HEK cells mainly represent an activation-independent feature of calcium channels due to the resting membrane potential of about −40 mV in HEK cells. In neurons, we employed an intracellular N-terminal tagged $Ca_V2.2$ channel (see below) to avoid any interference with the kinetic properties of the expressed channel population.

4.2 Single-Particle Tracking of Calcium Channel Subunits

To evaluate whether the differences in Ca^{2+} current densities and kinetics recorded from untagged and various tagged VGCCs reflect differences in the $\alpha_1/\alpha_2\delta_1$ interaction on the cell surface, we used SPT (Fig. 2). When we monitored the position and surface dynamics of VGCC by conjugating QDs with antibodies to tagged $Ca_V2.2$ pore-forming and $\alpha_2\delta_1$-subunits in this analysis (tagging schemes at left in Fig. 2), we observed that labeling densities varied between the different combinations of tagged channel subunits. Localization density maps and trajectories recorded from $Ca_V2.2$ channels and $\alpha_2\delta_1$-subunits expressed in different combinations show their distinct distributions in the membrane [Figs. 2(a)–2(d)]. We found that the surface expression of the extracellularly tagged $Ca_V2.2 :: GFP_{extra}$ channels strictly depends on the coexpression of an $\alpha_2\delta_1$-subunit. Moreover, HA-tagged $\alpha_2\delta_1$-subunits showed a rather diffusive localization with only a small population of clustered molecules when expressed alone [Fig. 2(a)], revealing a diffusion coefficient almost identical to GPI-anchored GFP [Fig. 2(e), items 1 and 2]. These results provide support for the proposed GPI-anchorage of $\alpha_2\delta$-subunits.[25] In contrast, coexpression of $\alpha_2\delta_1$ with either extra- or intracellularly GFP-tagged $Ca_V2.2$ channels (including the β_3-subunit as in all experiments) triggered the formation of surface clusters and partial confinement of $\alpha_2\delta_1$-subunits [Figs. 2(b)–2(d)]. While all $Ca_V2.2$ variants were able to cluster $\alpha_2\delta_1$, the restrictive effect of $Ca_V2.2$ on the mobility of $\alpha_2\delta_1$-subunit was stronger for the intracellularly tagged $Ca_V2.2$ channels compared to the extracellular variants [Fig. 2(e), items 3 versus 4]. Moreover, the extracellular GFP-tagged $Ca_V2.2$ channels themselves displayed significantly different surface mobility than intracellular tagged $Ca_V2.2$ channels [Fig. 2(e), items 5, 6]. Further tests with other channels ($Ca_V2.1$, $Ca_V1.2$, and $Ca_V3.2$) showed an isoform specific effect on the diffusion properties of $\alpha_2\delta_1$-subunits with different pore-forming α_1-subunits [Fig. 2(f)]. The low-voltage activated $Ca_V3.2$ channel did not induce a reduction of $\alpha_2\delta_1$-subunit surface dynamics [Fig. 2(f), item 6], whereas the surface trafficking of $Ca_V3.2$ channels is reported to be supported by the expression of $\alpha_2\delta_1$-subunits.[43]

We next used the extracellular tagged $Ca_V2.2$ channel to characterize the surface affinity between the two subunits. The labeling efficiency between extracellular HA-tagged and GFP-tagged $Ca_V2.2$ channels was substantially different. First, only coexpression of $Ca_V2.2$, β_3- and $\alpha_2\delta_1$-subunits was sufficient to bring a population of extracellular GFP-tagged $Ca_V2.2$ channels to the surface. Second, labeling efficiency was weaker for extracellular HA-tagged $Ca_V2.2$ channels than GFP-tagged $Ca_V2.2$ channels if all subunits are expressed. Third, the surface diffusion was significantly different between the two extracellular tagged $Ca_V2.2$ channels [Fig. 2(e), items 5, 6]. Probing the surface dynamics of $\alpha_2\delta_1$-subunits coexpressed with the extracellular tagged $Ca_V2.2$ channel is complementary to the dynamics of tagged $Ca_V2.2$ channels. Expression of $\alpha_2\delta_1$-subunits with extracellular GFP-tagged $Ca_V2.2$ channels slightly

Table 1 Activation and steady-state inactivation voltage of tagged and antibody labeled $Ca_V2.2$ channels expressed in HEK cells together with β_3- and $\alpha_2\delta_1$-subunits. Data are means $\pm$ SEM ($N = 5$ to 10 cells for each condition), significant changes are indicated as (*) in respect to the stable cell line.

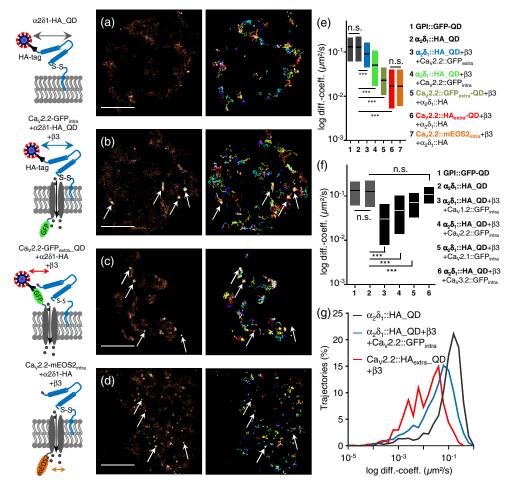| Plasmid combination	$V_{1/2active}$ (mV)	$V_{1/2inactive}$ (mV)
$Ca_V2.2 + \beta3 + \alpha_2\delta_1$ (stable cell line[27])	−10.7 ± 3.5	−70.4 ± 0.5
$Ca_V2.2 :: HA_{extra} + \beta3 + \alpha_2\delta_1$	−4.8 ± 2.9 (*)	−71.5 ± 0.2
$Ca_V2.2 :: HA_{extra} + \beta3 + \alpha_2\delta_1 +$ anti-HA antibody	−3.2 ± 4.1 (*)	−67.7 ± 0.4
$Ca_V2.2 :: GFP_{extra} + \beta3 + \alpha_2\delta_1$	−5.8 ± 3.7 (*)	−65.7 ± 0.4 (*)
$Ca_V2.2 :: GFP_{extra} + \beta3 + \alpha_2\delta_1 +$ anti-GFP antibody	−2.8 ± 3.1 (*)	−59.9 ± 0.2 (*)

Fig. 2 Surface dynamics of individual $Ca_V 2.2$ channel subunits and $\alpha_2\delta_1$-subunits expressed in different combinations. (a)–(d) Expressed combinations of $Ca_V 2.2$ and $\alpha_2\delta_1$-subunits in HEK cells and their localization density map as well as trajectory map are presented. The scale bar represents 500 nm. Arrows indicate clusters of the tracked subunit as indicated in the sketches on the left side. (e) Medians and interquatril range of diffusion coefficient of the mobile population of channel subunits in the cell membrane ($D > 0.001$ $\mu m^2/s$) for proteins and combinations as indicated. Data are from 2 to 3 transfected HEK-cell cultures, the number of trajectories are $\alpha_2\delta_1 + Ca_V 2.2::GFP_{extra}$: 1951, $\alpha_2\delta_1 + Cav2.2::GFP_{intra}$: 2223, $Ca_V 2.2::GFP_{extra}$: 1049, $Ca_V 2.2::HA_{extra}$: 279, $Ca_V 2.2::mEOS2_{intra}$: 8503 traj., significances were determined by a Kruskal–Wallis-test followed by a Dunn's multiple comparison test: **, $p < 0.005$; ***, $p < 0.0005$. (f) Median and interquatril range of diffusion coefficient of the mobile population ($D > 0.001$ $\mu m^2/s$) of $\alpha_2\delta_1$-subunit expressed alone or in combination with different $\alpha 1$-subunits as indicated. The number of trajectories are: GPI-GFP: 1172 traj., $\alpha 2\delta 1$: 8967 traj., $+\beta 3$ and $Ca_V 1.2$: 4609 traj., $+\beta 3$ and $Ca_V 2.2$: 6661 traj., $+\beta 3$ and $Ca_V 2.1$: 3558 traj., $+\beta 3$, and $Ca_V 3.2$: 563 traj.; (g) The distribution histogram for the diffusion coefficients of subunit combinations as indicated reveal the differences between the different combinations. Note that only a very small fraction of channels and subunits is indeed immobile ($D < 0.001$ $\mu m^2/s$).
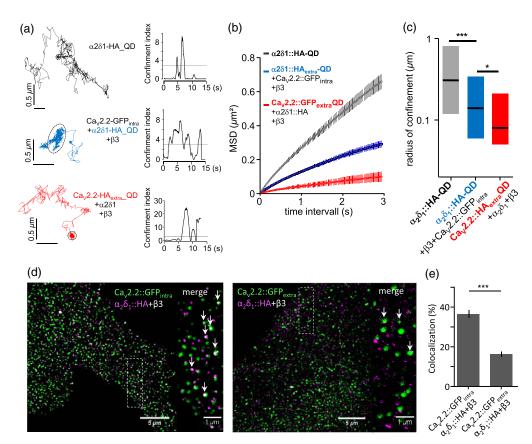
reduced the mobility of $\alpha_2\delta_1$-subunits. Whereas in combination with the intracellular GFP-tagged $Ca_V 2.2$ channel, the reduction of $\alpha_2\delta_1$-subunit surface dynamics was more prominent [Fig. 2(e), items 3, 4]. This indicates that $Ca_V 2.2$ channels are less mobile and more confined in the cell membrane than their associated $\alpha_2\delta_1$-subunits. Second, the association of the $\alpha_2\delta_1$-subunits is influenced by the extracellular tag of the $Ca_V 2.2$ channel, which might influence the voltage-dependent inactivation [Figs. 1(f) and 1(g)].[20] To assess whether the HA-tag within the $Ca_V 2.2$ channel affects its association with $\alpha_2\delta_1$, we expressed $Ca_V 2.2::HA_{extra}$ channels together with an FLAG-tagged $\alpha_2\delta_1$-subunit. The diffusion properties of the latter were similar to the HA-tagged $\alpha_2\delta_1$-subunit in combination with the intracellularly tagged channel $Ca_V 2.2::GFP_{intra}$ (data not

shown), implying that the HA-tag in the outer loops of $Ca_V 2.2$ channels has little if any impact on its association with $\alpha_2\delta_1$. Thus, the size of the extracellular label has a significant impact on the association of $Ca_V 2.2$ channels and $\alpha_2\delta_1$-subunits to each other. In addition, sptPALM experiments with N-terminal mEOS2 tagged $Ca_V 2.2$ channels support the diffusion dynamics recorded by the use of anti-HA-QD-labeled $Ca_V 2.2::HA_{extra}$ channels [Fig. 2(e), item 7]. These experiments exclude the possibility that antibody precoated QDs might have local cross-linking activity, which could influence surface dynamics of calcium channel subunits. The clustered distribution and slower diffusion of $Ca_V 2.2$ channels indicate a stronger confinement of the pore-forming subunit than the extracellular associated lipid anchored $\alpha_2\delta_1$-subunits.

Within long, reconnected single-particle trajectories periods of transient confinement are frequent. These observations indicate a dynamic association of channel subunits in the cell membrane [Fig. 3(a)]. The different diffusion behavior is visible in the distribution of the diffusion coefficient for $\alpha_2\delta_1$-subunits and $Ca_V2.2$ channels [Fig. 2(g)]. Plotting the MSD versus time interval [Fig. 3(b)] confirmed the idea of general stronger confinement of $Ca_V2.2$ channels versus $\alpha_2\delta_1$-subunits. Fitting the MSD of transient confined periods of diffusion [Fig. 3(a)], was used to determine the averaged surface of the explored area. The area of these transient confinements are different between the tested combinations as, $\alpha_2\delta_1$-subunit alone, $\alpha_2\delta_1$-subunits expressed together with intracellular tagged $Ca_V2.2$ channel and extracellular tagged $Ca_V2.2$ channels [Fig. 3(b)]. The differences in transient confinement strongly indicate a dynamic association of extracellular subunits with the pore forming subunits. Using dual color STED microscopy, we confirmed that there are changes in the colocalization of $Ca_V2.2$ channel and $\alpha_2\delta_1$-subunits, dependent on the position of the GFP-tag in the $Ca_V2.2$ channel [Figs. 3(d) and 3(e)]. Since the occupation rate of the tagged subunits and the respective antibody is not determined and might differ between the used epitopes (GFP-tag and HA-tag), this experiment does not allow to quantify the absolute ratio between associated and dissociated subunits. However, the relative difference in the colocalization indicate a mismatch in the case of extracellular GFP-tag on the $Ca_V2.2$ channel. Both dynamic and static imaging data indicate a fluctuation between associated and dissociated subunits. A potential mechanism to alter the kinetic properties of the surface expressed $Ca_V2.2$ channel population could be the up- or downregulation of surface expressed $\alpha_2\delta_1$-subunits, as seen in the development of chronic pain by nerve injuries in the peripheral nervous system.[44] However, an alteration in $\alpha_2\delta_1$-subunit expression is often accompanied by an overall change of the $Ca_V2.2$ channel expression as well.

4.3 Surface Mobility of Tagged $\alpha_2\delta_1$ VGCC Subunits in Neurons

To mitigate the limitations of a heterologous expression system, in particular, (i) the weak resting membrane potential of HEK293 cells causing a majority of expressed VGCCs to be
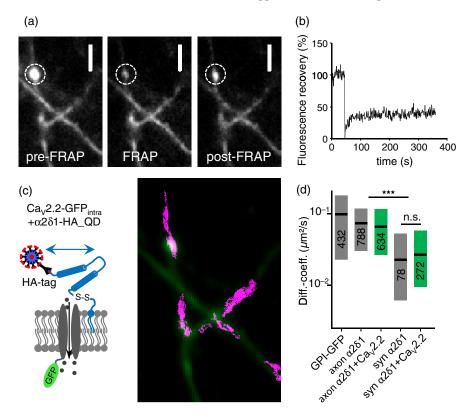

Fig. 3 Confinement of channel subunits depends on the interaction between $\alpha_2\delta_1$-subunit and $\alpha1$-subunit. (a) Example trajectories and confinement index over time for three subunit combinations as indicated, note the different time and height of confinement index. The dashed-circle indicates the temporal confinement of the tracked subunit. (b) Averaged MSDs over time interval for the constructs as indicated. Data are from 2 to 3 independent experiments $\alpha_2\delta_1::HA$: 393 trajectories, $\alpha_2\delta_1 + Ca_V2.2::GFP_{intra}$: 350 trajectories, $Ca_V2.2::GFP_{extra} + \alpha_2\delta_1::HA$: 138 trajectories. (c) Radius of confinement determined by fitting MSD curves during periods of confinement. Statistical tests used are one-way ANOVA followed by a posthoc Bonferroni-test. (d) STED images of $Ca_V2.2$ tagged intra- or extracellular with GFP and $\alpha_2\delta_1::HA$-subunits, note the only partial clustering of $Ca_V2.2$ and $\alpha_2\delta_1::HA$-subunits. Examples of colocalized clusters are indicated by the arrows. (e) Quantification of the population of $Ca_V2.2::GFP$ clusters colocalized with $\alpha_2\delta_1::HA$-subunit positive clusters, differences are tested by student's t-test, data are from three independent transfections of HEK cells, nine cells for each condition was analyzed with ~500 $Ca_V2.2::GFP$ clusters each.

in an inactivated state, (ii) the different lipid composition of the HEK293 membrane with putative effects on diffusion, and (iii) the different glycosylation pattern and entirely different spectrum of potential extracellular binding partners for $\alpha_2\delta_1$, we aimed to perform a proof-of-principle experiment in neurons (Fig. 4). To examine whether $Ca_V2.2$ and $\alpha_2\delta_1$-subunits also differ in their mobility in neuronal membranes, we expressed $Ca_V2.2 :: GFP_{intra}$ and $\alpha_2\delta_1$-HA in cultured hippocampal neurons. As mentioned above, extracellular tagged CaV2.2 channels did not express reliably in the neuronal membrane and had slightly altered kinetic properties, which was not the case for intracellular tagged channels. The use of $Ca_V2.2$ has the advantage that overexpression leads to their accumulation in the presynaptic compartment,[5,45,46] allowing us to probe whether $\alpha_2\delta_1$ show a tight association to pore-forming $Ca_V2.2$ subunits in a structurally defined membrane compartment. Intracellularly GFP-tagged $Ca_V2.2$ channels could be clearly detected in synapses [Fig. 4(a)]. We then used FRAP experiments to define the mobile fraction of $Ca_V2.2 :: GFP_{intra}$, resulting in 25% fluorescence recovery within 6 min after photobleach [Figs. 4(a) and 4(b)]. In addition, we monitored the surface dynamics of QD-labeled $\alpha_2\delta_1$-HA with and without coexpression of $Ca_V2.2 :: GFP_{intra}$. In neurons, the mobility of $\alpha_2\delta_1$-subunits in the axonal membrane was comparable to GPI::GFP [Fig. 4(d)], consistent with the HEK cell experiments [Fig. 2(f)]. In contrast to the heterologous expression system, the mobility of $\alpha_2\delta_1$-subunits on

the axonal membrane was not influenced by coexpression of $Ca_V2.2 :: GFP_{intra}$, even in the presynaptic membrane [Fig. 4(d); comparison to Figs. 2(e) and 2(f)]. More strikingly, however, the $\alpha_2\delta_1$-subunit dynamic is significantly different between the axonal and presynaptic membrane compartments [Fig. 4(d)], suggesting that in neurons, the localization of VGCCs affects the dynamics of subunits more than an association between subunits. In support, we observed that the majority of tagged molecules did not stabilize in the synapse but exchanged between the synaptic and extrasynaptic (axonal) membrane areas during the observation period [e.g., Fig. 4(c)]. As reported before, clustered $Ca_V2.2$ channels represent, to a large extent, presynaptic terminals.[5] Thus, these data support the observation in HEK293 cells that VGCC subunits are not tightly associated with each other on the cellular membrane. The strong effect of the localization (synaptic versus axonal) on diffusion, in turn, indicates that additional parameters involved in neurons remain to be uncovered in the future.

4.4 Modeling of Subunit Association Within Different Membrane Compartments

To systematically investigate whether the association between VGCC subunits depends on the level of overall surface expression or their local densities, we developed a modeling approach based on our previous work.[5] The model builds on

Fig. 4 Dynamics of channel subunits in the neuronal membrane. (a) Example for a FRAP experiment of $Ca_V2.2 :: GFP_{intra}$ channels expressed in hippocampal neurons 14 DIV, scale bare indicate 5 μm. (b) Example recovery curve of the region indicated in (a). The mean fluorescent recovery for $Ca_V2.2 :: GFP_{intra}$ channels was 24.8% $\pm$ 3% (data from 30 clusters analyzed out of 2 independent cultures). (c) Example traces for $\alpha_2\delta_1 :: HA$-subunits labeled with QDs as indicated in the sketch. (d) Medians of diffusion coefficients for GPI::GFP, $\alpha_2\delta_1 :: HA$-subunit alone, and $\alpha_2\delta_1 :: HA$-subunit coexpressed with $Ca_V2.2 :: GFP_{intra}$ channels in axonal and presynaptic membranes, as indicated. The number of trajectories is given for each condition and data are out of two independent experiments. The significance was tested by a Kruskal–Wallis test followed by a Dunns test to compare individual columns.
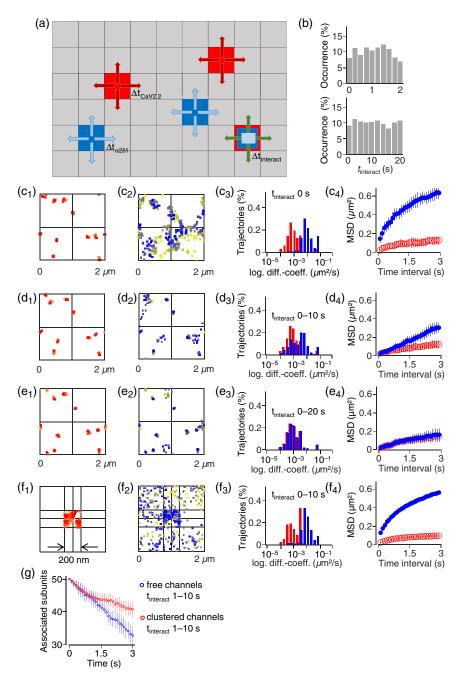
Fig. 5 Modeling interaction time of α_1- and $\alpha_2\delta_1$-subunits. (a) Part of a lattice grid used for the simulation with channel α_1 units (red), $\alpha_2\delta$ units (blue), and interacting channels and $\alpha_2\delta$ units (red–blue units in the top left part). (b) Random interaction time distribution for $t_{interact} \sim 1$ s and $t_{interact} \sim 10$ s as indicated. (C_{1-4}) Simulation of noninteracting channels and $\alpha_2\delta$-subunits: Trajectories of channels (1) and $\alpha_2\delta$-subunits (2), distribution of diffusion coefficient for channels (red) and $\alpha_2\delta$ units (blue) and averaged MSD of channels (red) and $\alpha_2\delta$-subunits (blue) over simulation time of 3s (4); (D_{1-4}) Simulation with interacting channels and $\alpha_2\delta$-subunits, interaction time corresponding to experimental observations, compare Fig. 3(b), black curve (display of data like in c); (E_{1-4}) Simulation of strongly interacting channels and $\alpha_2\delta$-subunits (display of data like in C); (F_{1-4}) Simulation on a smaller lattice grid were channels remain confined (200 nm × 200 nm), whereas $\alpha_2\delta$-subunits can enter and leave the area of channel confinement. The density of channels in the confinement is higher than in (c)–(e). The $\alpha_2\delta$-subunits are inserted within the channel confinement in a 1:1 initial ratio, whereas outside the channel cluster $\alpha_2\delta$-subunits are inserted in a similar density without channels. Association of the subunits is only possible in the confinement with box boundary conditions for the channels with interacting time between 0 and 10 s. (g) Number of pairs of interacting channel and $\alpha_2\delta$-subunits over simulation time of 3 s for the 2 μm × 2 μm lattice grid like case in (d) (blue) and smaller 200 nm × 200 nm lattice grid like in case (f), with the interaction time between 0 and 10 s.

a two-dimensional regular lattice [gray, Fig. 5(a)], in which α_1-[red, Fig. 5(a)] and $\alpha_2\delta_1$ [blue, Fig. 5(a)] subunits can occupy a number of positions with defined size of 10 nm × 10 nm. The subunits may move randomly in two dimensions [arrows, Fig. 5(a)], representing lateral diffusion within the cell membrane. The step time of the α_1-subunit Δt_{CaC} and the step time of the $\alpha_2\delta_1$-subunits $\Delta t_{\alpha2\delta1}$ correspond to the experimentally obtained diffusion coefficients (Fig. 2). Our model observes several limitations: (1) α_1-subunits and $\alpha_2\delta_1$-subunits do not occupy a position twice; (2) α_1 and $\alpha_2\delta_1$-subunits may occupy one lattice space together and then "interact" with each other [blue–red unit, Fig. 5(a)]; and (3) the system has open boundaries, thus α_1 and $\alpha_2\delta_1$-subunits can move across the lattice border and re-enter at the other side. If α_1 and $\alpha_2\delta_1$-subunits occupy the same position, they move together [green arrows, Fig. 5(a)] until a predefined interaction time $t_{interact}$ is reached and then they move again independently. We based our simulation in accordance with experimental observation data with 50 channels on a 2 μm × 2 μm system (corresponding to a 200 × 200 lattice grid) and added 50 units of a 1:1 ratio of $\alpha_2\delta_1$- to α_1-subunits, initially as interacting partners on the same squares. We set the interaction time $t_{interact}$ between a α_1 and $\alpha_2\delta_1$ pairs as an equal-distributed number with a defined mean value [Fig. 5(b) shows $t_{interact}$ distributions for mean values of $t_{interact} \sim$ 10 s and $t_{interact} \sim 1$ s]. Thus, the variable parameter in our Monte Carlo simulation is the interaction time of channels and $\alpha_2\delta_1$-subunits.

The first simulation shows the results for noninteracting α_1 and $\alpha_2\delta_1$-subunits, i.e., a system with an interaction time $t_{interact} = 0$ s [Fig. 5(c$_{1-4}$)]. The display represents 10 trajectories of channels [Fig. 5(c$_1$)] and 10 $\alpha_2\delta_1$-subunits [Fig. 5(c$_2$)]. The trajectory selection is done to enhance the visibility of particular channel trajectories but is random. The color code change is from orange (starting position) to red (final position) for channels, and from yellow (starting position) to blue (final position) for $\alpha_2\delta_1$-subunits. The Monte Carlo simulations were repeated 20 times, a sufficient number to obtain a robust distribution of diffusion coefficients. As shown in Fig. 5(c$_{3-4}$)diffusion coefficients and MSD curves are very different from channels and $\alpha_2\delta_1$-subunits and comparable to the mobility properties if both proteins are expressed seperately.

We next assumed an interaction time between 0 and 10 s for channels and $\alpha_2\delta_1$-subunits, resulting in a simulation of diffusion coefficients and MSD for $\alpha_2\delta_1$-subunit and channels that overlap and are close to the experimental situation [Fig. 5(d$_{1-4}$)], [see Fig. 2(b), blue line and Fig. 3(b), blue curve]. Interestingly, increasing the range of the interaction time 0 to 20 s led to an almost identical mobility of channels and $\alpha_2\delta_1$-subunits [Fig. 5(e$_{1-4}$)]. Thus, we kept the value of $t_{interact}$ between 0 and 10 s to simulate our experimental conditions. Short interaction times between 0 and 1 s between $\alpha_2\delta_1$-subunits and channels lead to a diffusion coefficient distribution which was broader. The empirically found time window for subunit interactions (0 to 10 s) should help to simulate the distribution and interaction times in the presynaptic membrane.

Finally, we studied the situation of calcium channels in the presynaptic membrane where their density is presumably much higher.[5] We simulated a confined presynaptic membrane (200 nm × 200 nm) within the area used before (2 μm × 2 μm) and concentrated all 50 channels into the confinement [Fig. 5(f$_1$)]. We assumed that channels are confined in this small area, but allowed $\alpha_2\delta_1$-subunits to move independently in and out of the

confined area. The start point for the simulation was that both channels and $\alpha_2\delta_1$-subunits are placed in the confined area. Due to the liberty of $\alpha_2\delta_1$-subunits, no $\alpha_2\delta_1$-subunit remains bound to a channel, which is a situation similar to 0 s interaction time (data not shown). We balanced this effect by increasing the number of $\alpha_2\delta_1$-subunits in the periphery of the channel cluster to equalize the density outside the confinement of the channels [Fig. 5(f$_{1-4}$)]. Now, the mobility of channels was slightly reduced within the confinement [Fig. 5(f$_{3-4}$)] compared to the larger 2 μm × 2 μm system [Figs. 5(c)–5(e)]. The diffusion properties of $\alpha_2\delta_1$-subunits were also altered since the majority of the $\alpha_2\delta_1$-subunits can move freely without α_1-subunit interactions. A small part of the $\alpha_2\delta_1$-subunits bound to channels remain partially in the central area [Fig. 5(f$_2$)]. This is also reflected in the small subpopulation of slower $\alpha_2\delta_1$-subunits in the distribution of the diffusion coefficient [Fig. 5(f$_3$)]. The simulation predicts that under all conditions tested there will be a population of channels in the synapse lacking an $\alpha_2\delta_1$-subunit. In order to illustrate the fraction of free channels, we counted the number of interacting pairs over time for two systems with the interaction time resulting in the diffusion properties as seen in our experiments ($t_{interact}$ 0 to 10 s). For the 2 μm × 2 μm system [Fig. 5(d)], the number of $\alpha_2\delta$-subunit-associated channels continuously decreased. For channels confined into the smaller 200 nm × 200 nm system [Fig. 5(f)] and with an excess of exchanging $\alpha_2\delta_1$-subunits, the population of $\alpha_2\delta$-subunit-associated channels reached a plateau after 1 to 2 s [Fig. 5(g)]. These results indicate that confinement of channels and the overpopulation of $\alpha_2\delta_1$-subunits might be sufficient to regulate surface channel assembly, despite the low affinity of Ca$_V$2.2 channel and $\alpha_2\delta_1$-subunits.

5 Discussion

Function and assembly of VGCCs have been studied intensely in heterologous expression systems and depend critically on the association of α_1 pore-forming with auxiliary β- and $\alpha_2\delta$-subunits.[8] While β-subunits are absolutely required for the trafficking of α_1 pore-forming subunits to the plasma cell membrane, $\alpha_2\delta$-subunits are able to further enhance the forward trafficking to promote a stronger surface expression of the channel.[8,11] In addition, isoforms of both β- and $\alpha_2\delta$-subunits have different impacts on the kinetic properties of VGCCs.[7] The study of the role of auxiliary VGCC subunits has been confounded by the observation that in neurons, at least $\alpha_2\delta$-subunits have additional roles.[13,16]

Most of the experiments in our study focused on the surface interaction of VGCC with $\alpha_2\delta_1$-subunits. Their interaction is particularly important for the activation of VGCC[20,47] during the development of chronic pain[26,48] and synaptogenesis,[16] where the Ca$_V$2.2 channels are particularly the dominant calcium channel in immature hippocampal glutamatergic synapses.[49] Probing the dynamics of the two subunits showed that Ca$_V$2.2 channels and $\alpha_2\delta_1$-subunits are not permanently associated but rather transiently associate in both HEK293 cells and neurons. Using extracellular and intracellular tagged Ca$_V$2.2 channels and $\alpha_2\delta_1$-subunits revealed the existence of three populations: free Ca$_V$2.2 channels, free $\alpha_2\delta_1$-subunits, and associated Ca$_V$2.2 channels with $\alpha_2\delta_1$-subunits. If there will indeed be a 1:1:1 stoichiometry between the channel subunits,[6,18] the weak affinity (dwell time/$t_{interact}$) might be compensated by different expression levels and confinement of subunits in the membrane, particular in synapses. Comparing the dynamics of both subunits [Figs. 2(e) and 2(g), 4(a)–4(d), 5(a)–5(d)] confirmed a substantial difference in

the confinement of $Ca_V2.2$ channels and $\alpha_2\delta_1$-subunits [Figs. 3(b) and 3(c), 4(a)–4(d), 5(a)–5(d)]. This observation was further substantiated by determining the colocalization of calcium channel subunits in the plane of the cell membrane using STED microscopy [Figs. 3(d) and 3(e)]. The physiological consequences are proposed by the altered voltage-dependent inactivation of evoked barium currents from tagged channels where the interaction between $Ca_V2.2$ channels and $\alpha_2\delta_1$-subunits is altered [$Ca_V2.2 :: GFP_{extra}$, Fig. 1(d)]. Whether the dynamic subunit associations will be a mechanism that influences channel activity in their natural environment needs to be further explored. Interestingly, the affinity of α_1-subunits and $\alpha_2\delta_1$-subunits seems to be different between different calcium channels as observed in the altered diffusion coefficient of $\alpha_2\delta_1$-subunits when expressed with $Ca_V1.2$, $Ca_V2.2$, $Ca_V2.1$, or $Ca_V3.2$ channels [Fig. 2(f)]. The strongest association seems to exist between $Ca_V1.2$ and $\alpha_2\delta_1$-subunits, whereas $Ca_V3.2$ channels do not seem to interact with $\alpha_2\delta_1$-subunits at the cell surface. With respect to the physiological channel function and subunit association, $\alpha_2\delta_1$-subunits are identified to tune the voltage-dependent opening of $Ca_V1.2$ channels.[20,47,50] Recently, the first crystal structure of the $Ca_V1.1$ channel complex has been described by the use of cryo-electron microscopy. Here, the authors demonstrate that the interface of binding between $Ca_V1.1$ and $\alpha_2\delta_1$-subunit is between the extracellular loops of the transmembrane repeats I–III and the von Willebrand A domain and cache1 domain of the $\alpha_2\delta_1$-subunit.[18] Using voltage clamp fluorometry, it has been shown that the channel $\alpha_2\delta_1$-subunit interaction with the voltage sensor domains within the transmembrane repeats I–III is relevant for the activation of the channel.[20] In light of these recent structure-function data, we cannot fully exclude that the tagging of the $\alpha_2\delta_1$-subunit on the N-terminus will influence the association of the subunits. However, the functional tests with and without HA-tagged $\alpha_2\delta_1$-subunits (Fig. 1) speak against a major impact of the chosen tag position. Whether the proposed dynamic association between $\alpha_2\delta_1$-subunits and $Ca_V2.2$ channels will be of functional relevance in neurons has to be tested. In specific compartments, the synapse channel densities can be tenfold higher[5,51,52] as in the axon controlled by many molecular interactions.[53] Our first data in neurons suggest that $\alpha_2\delta_1$-subunits are more confined in synapses, which is rather due to other interactions than a specific affinity to $Ca_V2.2$ channels (Fig. 4). The interaction with extracellular matrix proteins[16,54] might be effective to confine $\alpha_2\delta_1$-subunits in the synapse. Our simulations suggest that such local molecular crowding has an impact on the association of channel subunits. The simulation further indicated that the copy numbers for channels and $\alpha_2\delta_1$-subunits should be very different to have a certain population of $\alpha_2\delta_1$-subunits bound to the channels. The confinement and increased density of $Ca_V2.2$ channels themselves can be assigned to many intracellular interaction partners, particularly in the synapse.[55–58] Whether other molecules, e.g., synaptic adhesion proteins such as neurexins,[59] participate in the confinement of channels or $\alpha_2\delta_1$-subunits remains to be tested.

Thus, the described differences in surface dynamics of channel subunits give potential new insights into the function of calcium channels. The labile interaction between channel and $\alpha_2\delta$-subunits suggests a local and fast mechanism to alter the signaling capacity of calcium channels based on their subunit composition. The timescale for such altered interactions are in the range of milliseconds to seconds and could represent a potential variable tuning voltage-dependent calcium signaling.

References

1. B. A. Simms and G. W. Zamponi, "Neuronal voltage-gated calcium channels: structure, function, and dysfunction," *Neuron* **82**(1), 24–45 (2014).
2. E. Eggermann et al., "Nanodomain coupling between Ca^{2+} channels and sensors of exocytosis at fast mammalian synapses," *Nat. Rev. Neurosci.* **13**(1), 7–21 (2012).
3. M. R. Tadross, R. W. Tsien, and D. T. Yue, "Ca^{2+} channel nanodomains boost local Ca^{2+} amplitude," *Proc. Natl. Acad. Sci. U. S. A.* **110**(39), 15794–15799 (2013).
4. Y. Nakamura et al., "Nanoscale distribution of presynaptic Ca(2+) channels and its impact on vesicular release during development," *Neuron* **85**(1), 145–158 (2015).
5. R. Schneider et al., "Mobility of calcium channels in the presynaptic membrane," *Neuron* **86**(3), 672–679 (2015).
6. W. A. Catterall, "Voltage-gated calcium channels," *Cold Spring Harb. Perspect. Biol.* **3**(8), a003947 (2011).
7. M. Campiglio and B. E. Flucher, "The role of auxiliary subunits for the functional diversity of voltage-gated calcium channels," *J. Cell Physiol.* **230**(9), 2019–2031 (2015).
8. A. C. Dolphin, "Calcium channel auxiliary alpha2delta and beta subunits: trafficking and one step beyond," *Nat. Rev. Neurosci.* **13**(8), 542–55 (2012).
9. S. Geisler, C. L. Schopf, and G. J. Obermair, "Emerging evidence for specific neuronal functions of auxiliary calcium channel alpha(2)delta subunits," *Gen. Physiol. Biophys.* **34**(2), 105–118 (2015).
10. M. Xie et al., "Facilitation versus depression in cultured hippocampal neurons determined by targeting of Ca^{2+} channel Cavbeta4 versus Cavbeta2 subunits to synaptic terminals," *J. Cell Biol.* **178**(3), 489–502 (2007).
11. N. Klugbauer et al., "Molecular diversity of the calcium channel alpha2-delta subunit," *J. Neurosci.* **19**(2), 684–691 (1999).
12. I. Kadurin et al., "Calcium currents are enhanced by alpha2delta-1 lacking its membrane anchor," *J. Biol. Chem.* **287**(40), 33554–33566 (2012).
13. M. B. Hoppa et al., "Alpha2delta expression sets presynaptic calcium channel abundance and release probability," *Nature* **486**(7401), 122–125 (2012).
14. M. D'Arco et al., "The upregulation of alpha2delta-1 subunit modulates activity-dependent Ca^{2+} signals in sensory neurons," *J. Neurosci.* **35**(15), 5891–5903 (2015).
15. P. T. Kurshan, A. Oztan, and T. L. Schwarz, "Presynaptic alpha2delta-3 is required for synaptic morphogenesis independent of its Ca^{2+}-channel functions," *Nat. Neurosci.* **12**(11), 1415–1423 (2009).
16. C. Eroglu et al., "Gabapentin receptor alpha2delta-1 is a neuronal thrombospondin receptor responsible for excitatory CNS synaptogenesis," *Cell* **139**(2), 380–392 (2009).
17. S. Vergult et al., "Genomic aberrations of the CACNA2D1 gene in three patients with epilepsy and intellectual disability," *Eur. J. Hum. Genet.* **23**(5), 628–632 (2015).
18. J. Wu et al., "Structure of the voltage-gated calcium channel Cav1.1 complex," *Science* **350**(6267), aad2395 (2015).
19. C. Canti et al., "The metal-ion-dependent adhesion site in the Von Willebrand factor-A domain of alpha2delta subunits is key to trafficking voltage-gated Ca^{2+} channels," *Proc. Natl. Acad. Sci. U. S. A.* **102**(32), 11230–11235 (2005).
20. N. Savalli et al., "The alpha2delta-1 subunit remodels CaV1.2 voltage sensors and allows Ca^{2+} influx at physiological membrane potentials," *J. Gen. Physiol.* **148**(2), 147–159 (2016).

21. M. P. Tetreault et al., "Identification of glycosylation sites essential for surface expression of the CaValpha2delta1 subunit and modulation of the cardiac CaV1.2 channel activity," *J. Biol. Chem.* **291**(9), 4826–4843 (2016).
22. C. A. Gurnett, R. Felix, and K. P. Campbell, "Extracellular interaction of the voltage-dependent Ca²⁺ channel alpha2delta and alpha1 subunits," *J. Biol. Chem.* **272**(29), 18508–18512 (1997).
23. C. S. Muller et al., "Quantitative proteomics of the Cav2 channel nanoenvironments in the mammalian brain," *Proc. Natl. Acad. Sci. U. S. A.* **107**(34), 14950–14957 (2010).
24. P. Robinson et al., "Targeting of voltage-gated calcium channel alpha2-delta-1 subunit to lipid rafts is independent from a GPI-anchoring motif," *PLoS One* **6**(6), e19802 (2011).
25. A. Davies et al., "The alpha2delta subunits of voltage-gated calcium channels form GPI-anchored proteins, a posttranslational modification essential for function," *Proc. Natl. Acad. Sci. U. S. A.* **107**(4), 1654–1659 (2010).
26. S. Heyes et al., "Genetic disruption of voltage-gated calcium channels in psychiatric and neurological disorders," *Prog. Neurobiol.* **134**, 36–54 (2015).
27. Y. Lin, S. I. McDonough, and D. Lipscombe, "Alternative splicing in the voltage-sensing region of N-Type CaV2.2 channels modulates channel kinetics," *J. Neurophysiol.* **92**(5), 2820–2830 (2004).
28. G. J. Obermair et al., "Reciprocal interactions regulate targeting of calcium channel beta subunits and membrane expression of alpha1 subunits in cultured hippocampal neurons," *J. Biol. Chem.* **285**(8), 5776–5791 (2010).
29. M. Heine et al., "Surface mobility of postsynaptic AMPARs tunes synaptic transmission," *Science* **320**(5873), 201–205 (2008).
30. L. Groc et al., "Surface trafficking of neurotransmitter receptor: comparison between single-molecule/quantum dot strategies," *J. Neurosci.* **27**(46), 12433–12437 (2007).
31. A. Serge et al., "Receptor activation and homer differentially control the lateral mobility of metabotropic glutamate receptor 5 in the neuronal membrane," *J. Neurosci.* **22**(10), 3910–3920 (2002).
32. I. Izeddin et al., "Wavelet analysis for single molecule localization microscopy," *Opt. Express* **20**(3), 2081–2095 (2012).
33. V. Racine et al., "Multiple target tracking of 3D fluorescent objects based on simulated annealing," in *Proc. of the IEEE Int. Symp. on Biomedical Imaging (ISBI'2006)*, pp. 1020–1023 (2006).
34. P. Annibale et al., "Quantitative photo activated localization microscopy: unraveling the effects of photoblinking," *PLoS One* **6**(7), e22678 (2011).
35. A. Kusumi, Y. Sako, and M. Yamamoto, "Confined lateral diffusion of membrane receptors as studied by single particle tracking (nanovid microscopy). Effects of calcium-induced differentiation in cultured epithelial cells," *Biophys. J.* **65**(5), 2021–2040 (1993).
36. C. Altier et al., "ORL1 receptor-mediated internalization of N-type calcium channels," *Nat. Neurosci.* **9**(1), 31–40 (2006).
37. J. S. Cassidy et al., "Functional exofacially tagged N-type calcium channels elucidate the interaction with auxiliary alpha2delta-1 subunits," *Proc. Natl. Acad. Sci. U. S. A.* **111**(24), 8979–8984 (2014).
38. V. Di Biase et al., "Surface traffic of dendritic CaV1.2 calcium channels in hippocampal neurons," *J. Neurosci.* **31**(38), 13682–13694 (2011).
39. C. Altier et al., "Trafficking of L-type calcium channels mediated by the postsynaptic scaffolding protein AKAP79," *J. Biol. Chem.* **277**(37), 33598–33603 (2002).
40. G. J. Obermair et al., "Differential targeting of the L-type Ca²⁺ channel alpha 1C (CaV1.2) to synaptic and extrasynaptic compartments in hippocampal neurons," *Eur. J. Neurosci.* **19**(8), 2109–2122 (2004).
41. I. E. Michailidis et al., "Age-related homeostatic midchannel proteolysis of neuronal L-type voltage-gated Ca²⁺ channels," *Neuron* **82**(5), 1045–1057 (2014).
42. K. Watschinger et al., "Functional properties and modulation of extracellular epitope-tagged Ca(V)2.1 voltage-gated calcium channels," *Channels* **2**(6), 461–473 (2008).
43. S. J. Dubel et al., "Plasma membrane expression of T-type calcium channel alpha(1) subunits is modulated by high voltage-activated auxiliary subunits," *J. Biol. Chem.* **279**(28), 29263–29269 (2004).
44. C. S. Bauer et al., "The increased trafficking of the calcium channel subunit alpha2delta-1 to presynaptic terminals in neuropathic pain is inhibited by the alpha2delta ligand pregabalin," *J. Neurosci.* **29**(13), 4076–4088 (2009).
45. A. Maximov and I. Bezprozvanny, "Synaptic targeting of N-type calcium channels in hippocampal neurons," *J. Neurosci.* **22**(16), 6939–6952 (2002).
46. Y. Q. Cao and R. W. Tsien, "Different relationship of N- and P/Q-type Ca²⁺ channels to channel-interacting slots in controlling neurotransmission at cultured hippocampal synapses," *J. Neurosci.* **30**(13), 4536–4546 (2010).
47. P. Tuluc et al., "Computer modeling of siRNA knockdown effects indicates an essential role of the Ca²⁺ channel alpha2delta-1 subunit in cardiac excitation-contraction coupling," *Proc. Natl. Acad. Sci. U. S. A.* **104**(26), 11091–11096 (2007).
48. K. W. Li et al., "Calcium channel alpha2delta1 proteins mediate trigeminal neuropathic pain states associated with aberrant excitatory synaptogenesis," *J. Biol. Chem.* **289**(10), 7025–7037 (2014).
49. K. P. Scholz and R. J. Miller, "Developmental changes in presynaptic calcium channels coupled to glutamate release in cultured rat hippocampal neurons," *J. Neurosci.* **15**(6), 4612–4617 (1995).
50. G. J. Obermair et al., "The Ca²⁺ channel alpha2delta-1 subunit determines Ca²⁺ current kinetics in skeletal muscle but not targeting of alpha1S or excitation-contraction coupling," *J. Biol. Chem.* **280**(3), 2229–2237 (2005).
51. N. Holderith et al., "Release probability of hippocampal glutamatergic terminals scales with the size of the active zone," *Nat. Neurosci.* **15**(7), 988–997 (2012).
52. D. W. Indriati et al., "Quantitative localization of Cav2.1 (P/Q-type) voltage-dependent calcium channels in Purkinje cells: somatodendritic gradient and distinct somatic coclustering with calcium-activated potassium channels," *J. Neurosci.* **33**(8), 3668–3678 (2013).
53. W. A. Catterall and A. P. Few, "Calcium channel regulation and presynaptic plasticity," *Neuron* **59**(6), 882–901 (2008).
54. B. Lana et al., "Thrombospondin-4 reduces binding affinity of [(3)H]-gabapentin to calcium-channel alpha2delta-1-subunit but does not interact with alpha2delta-1 on the cell-surface when co-expressed," *Sci. Rep.* **6**, 24531 (2016).
55. J. Rettig et al., "Alteration of Ca²⁺ dependence of neurotransmitter release by disruption of Ca²⁺ channel/syntaxin interaction," *J. Neurosci.* **17**(17), 6647–6656 (1997).
56. C. Acuna et al., "RIM-BPs mediate tight coupling of action potentials to Ca(2+)-triggered neurotransmitter release," *Neuron.* **87**(6), 1234–1247 (2015).
57. H. Hibino et al., "RIM binding proteins (RBPs) couple Rab3-interacting molecules (RIMs) to voltage-gated Ca(2+) channels," *Neuron* **34**(3), 411–423 (2002).
58. P. S. Kaeser et al., "RIM proteins tether Ca²⁺ channels to presynaptic active zones via a direct PDZ-domain interaction," *Cell* **144**(2), 282–295 (2011).
59. M. Missler et al., "Alpha-neurexins couple Ca²⁺ channels to synaptic vesicle exocytosis," *Nature* **423**(6943), 939–948 (2003).

Andreas Voigt received his PhD in theoretical physics from Otto-von-Guericke University Magdeburg, Germany. He pursued a career in modeling and simulation starting as a postdoc at the Center for Simulational Physics, University of Georgia, USA. At the Max-Planck-Institute for Dynamics of Complex Technical Systems Magdeburg, he continued to explore options for computer simulations now in chemical and biotechnological applications and is currently a lecturer and researcher in the Systems and Process Engineering Department of the University of Magdeburg.

Romy Freund received her Diploma degree in biochemistry from the Martin Luther University Halle-Wittenberg, Germany. Afterward, she did her PhD in the Research Group Molecular Physiology of Martin Heine, Leibniz Institute of Neuroscience, Magdeburg, about calcium channel mobility in the neuronal membrane.

Jennifer Heck received her BSc and MSc degrees in biosystems engineering from the Otto-von-Guericke-University, Magdeburg, Germany, in 2014 and 2016, respectively. In 2012, she joined the Research Group Molecular Physiology, Leibniz-Institute for Neurobiology, Magdeburg, Germany, headed by Dr. Martin Heine, as a scientific assistant. Here, she started her PhD project on the topic of voltage-gated calcium channel surface dynamics in the presynaptic compartment in April 2016.

Markus Missler studied medicine and philosophy at the University of Göttingen, Germany, and University of London, UK. After his doctoral thesis on synaptogenesis in the visual cortex of marmoset monkeys, he started to work on synaptic cell adhesion molecules such as

neurexins and ligands as a postdoctoral fellow in Thomas Südhof's Laboratory, Southwestern Medical Center, Dallas, Texas, USA. Currently, he is a full professor of anatomy and molecular neurobiology at the University of Münster, Germany.

Gerald J. Obermair studied zoology and neuroscience in Salzburg, Austria, and Ohio (USA). He did his PhD thesis on neuronal calcium regulatory proteins at the University of Innsbruck, Austria. In 2010, he completed his habilitation (Venia docendi) in physiology. Since 2013, he has been an associate professor at the Division of Physiology at the Medical University of Innsbruck. His research aims at understanding the functional heterogeneity of neuronal calcium channels and their involvement in neuronal disease.

Ulrich Thomas did his PhD at the Institute for Developmental Biology, Cologne, under supervison of Elisabeth Knust. With a background in molecular biology and genetics, he joined Eckart Gundelfinger's Group, Institute for Neurobiology, Magdeburg. Since then and during a postdoc research stay in Vivian Budnik's Lab, USA, his research focused on scaffold proteins, cell adhesion molecules, and calcium pumps at glutamatergic synapses in Drosophila.

Martin Heine received his PhD in zoology from the University of Göttingen. As a postdoc in the group of Daniel Choquet, University of Bordeaux, France, he investigated the surface dynamics and physiological impact of receptor and adhesion molecules in synapses. After that, he moved to the Leibniz-Institute for Neurobiology, Magdeburg, Germany. His research focuses on the dynamic organization of ion channels and adhesion molecules as a source of synaptic variability and short-term plasticity.